IEEE Access
Multidisciplinary | Rapid Review | Open Access Journal

Received February 10, 2020, accepted March 1, 2020, date of publication March 5, 2020, date of current version March 20, 2020.

Digital Object Identifier 10.1109/ACCESS.2020.2978545

Dual-Band Negative Group Delay Microwave Circuit With Low Signal Attenuation and Arbitrary Frequency Ratio

YUWEI MENG[1], ZHONGBAO WANG[1,2], (Member, IEEE), SHAOJUN FANG[1], (Member, IEEE), TE SHAO[1], HONGMEI LIU[1], (Member, IEEE), AND ZHINING CHEN[2], (Fellow, IEEE)

[1]School of Information Science and Technology, Dalian Maritime University, Dalian 116026, China
[2]Department of Electrical and Computer Engineering, National University of Singapore, Singapore 117583

Corresponding author: Zhongbao Wang (wangzb@dlmu.edu.cn)

This work was supported in part by the National Natural Science Foundation of China under Grant 61871417, Grant 51809030, and Grant 61571075, in part by the Natural Science Foundation of Liaoning Province under Grant 2019-MS-024, in part by the Youth Science and Technology Star Project Support Program of Dalian City under Grant 2016RQ038, and in part by the Fundamental Research Funds for the Central Universities under Grant 3132019219 and Grant 3132019211.

ABSTRACT A dual-band negative group delay (NGD) microwave circuit with low signal-attenuation and arbitrary frequency ratio is proposed. Closed-form analytical equations are derived for the design of the proposed dual-band negative group delay circuit (NGDC) with the variable frequency ratio. The characteristic parameters of the microstrip lines that influence the frequency ratio are investigated. Under the condition that the microstrip circuit can be implemented with the common printed circuit board (PCB) fabrication technology, the frequency ratio can vary between 1.1 and 6.3. For verification, three dual-band NGDCs with the frequency ratio of 1.105, 3, and 5.667 are designed, fabricated, and measured. Good agreements are observed between simulated and measured results, indicating the validity of the proposed methods.

INDEX TERMS Arbitrary frequency ratio, dual-band microwave circuit, low signal-attenuation, negative group delay.

I. INTRODUCTION

Modern wireless communication systems are required to operate at several frequency bands and work across different communication standards. Therefore, more than one of the single-frequency devices are used, which result in complex circuit structure and large size. So, multiband circuit components need to be used to reduce the system complexity and circuit size [1]–[3]. Moreover, the group delay (GD) has attracted a lot of attention because the variation of GD can cause dispersion and non-identity of the output in ultra-wideband applications [4]. Therefore, negative group delay (NGD) compensation circuits [5]–[8] are needed to equalize the delay. The negative group delay circuit (NGDC) is first proposed in [9]. And the NGD characteristics could be generated by RLC resonant circuits [10] or left-handed materials [11]. Based on the mode of transmission, the NGDCs can be divided into two categories: the reflection type and the transmission type. For the reflection type, the couplers are usually needed to transform the circuit into transmission type [12]–[15]. Therefore these circuits are often oversized. For the transmission types [16], [17], additional components are not required but the energy consumption is severe. Then some passive circuits or structures based on the amplifier are presented to reduce the insertion loss (IL) [18]–[23]. However, these circuits only operate at one frequency and are incompetent for multiband application. In [24], a dual-band NGDC with the right/left-handed transmission line is proposed. Nevertheless, it still needs to use couplers and has a significant decrease in signal. In order to realize miniaturization, some novel circuits are presented [25]–[28]. In [25], it is using dual-plane defected structures to generate dual-band NGD. However, the dimensions of the structure cannot be calculated. In [26], a couple of $\lambda_g/4$ open-circuited stubs are utilized, but it suffers high IL and the port matching cannot be obtained. For [27], [28], although the size is reduced by meandering transmission lines, the loss is still considerable. So the active dual-band NGDC is put forward

The associate editor coordinating the review of this manuscript and approving it for publication was Dušan Grujić.

to achieve gain compensation [29]. However, all the circuits in [24]–[29] are unable to achieve the frequency ratio greater than 3.

In this paper, a dual-band NGDC with arbitrary frequency ratio is proposed to reduce the signal attenuation. The proposed NGDC consists of two one-port open-circuited coupled lines, a resistor $R_{\rm m}$ connected by two transmission lines, and an open-circuited stub (or a short-circuited stub) connecting with two resistors R. The frequency ratio is mainly controlled by the coupling coefficient of the coupled lines and the characteristic impedance of the stub. And a wider range of frequency ratios can be obtained by using different stubs.

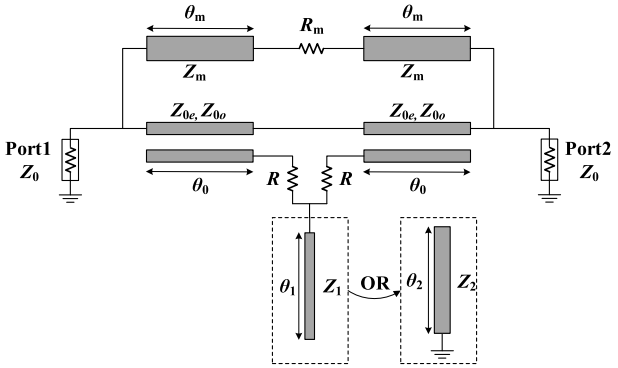

FIGURE 1. Configuration of the proposed NGD microwave circuit.

II. THEORY AND DESIGN EQUATION

The proposed NGDC topology is shown in Fig. 1. It is composed of a resistor $R_{\rm m}$ inserted between two transmission lines with characteristic impedance $Z_{\rm m}$ and electrical length $\theta_{\rm m}$, two one-port open-circuited coupled lines with even- and odd-mode characteristic impedance $Z_{0\rm e}$, $Z_{0\rm o}$ and electrical length θ_0, and an open-circuited stub with characteristic impedance Z_1 and electrical length θ_1 (or a short-circuited stub with characteristic impedance Z_2 and electrical length θ_2) connecting with two resistors R. The even- and odd-mode characteristic impedances of the coupled lines are calculated with Equation (1).

$$Z_{0\rm e} = Z\sqrt{\frac{1+k}{1-k}}, \tag{1a}$$

$$Z_{0\rm o} = Z\sqrt{\frac{1-k}{1+k}}. \tag{1b}$$

where Z and k represent the characteristic impedance and the coupling coefficient of the coupled line, respectively. The couple lines are used to reduce signal attenuation, and the different forms of the stub can achieve a wider range of frequency ratios.

As for analyzing, the even- and odd-mode equivalent circuits are shown in Fig. 2. According to [30], the different forms of coupling lines can be discussed. And based on transmission line theory and network analysis, the even- and

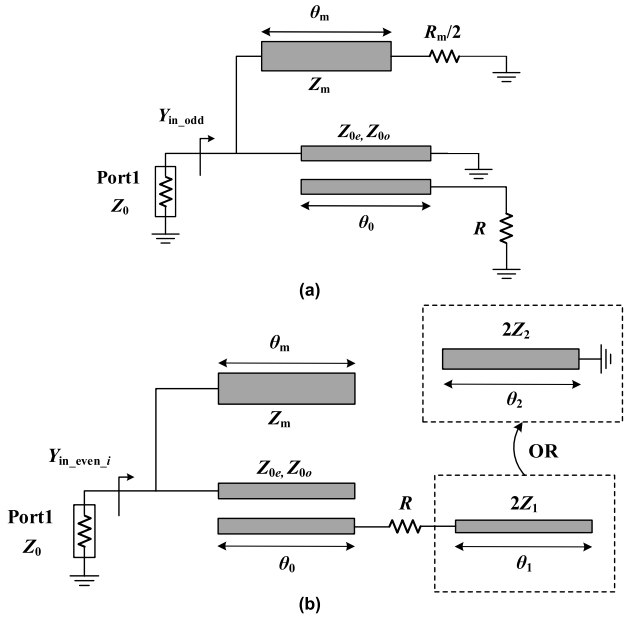

FIGURE 2. Odd- and even-mode equivalent circuits. (a) Odd-mode. (b) Even-mode.

odd-mode input admittance $Y_{\rm in\_odd}$ and $Y_{\rm in\_even\_}i$ are expressed as

$$Y_{\rm in\_odd} = A_1 + {\rm j}A_2, \tag{2a}$$

$$Y_{\rm in\_even\_}i = A_{3i} + {\rm j}A_{4i} \quad (i = 1, 2), \tag{2b}$$

where $i = 1$ represents the circuit with the open-circuited stub, $i = 2$ represents the circuit with the short-circuited stub. This representation is also applicable to subsequent derivation. And the expressions of A_1, A_2, A_{3i}, and A_{4i} in the Equations (2a) and (2b) could be found in the Appendix. Once the $Y_{\rm in\_odd}$ and $Y_{\rm in\_even\_}i$ are obtained, the S-parameters of the dual-band NGD microwave circuit can be expressed as [31]

$$S_{11\_}i = S_{22\_}i = \frac{Y_0^2 - Y_{\rm in\_odd}Y_{\rm in\_even\_}i}{\left(Y_0 + Y_{\rm in\_odd}\right)\left(Y_0 + Y_{\rm in\_even\_}i\right)}, \tag{3a}$$

$$S_{12\_}i = S_{21\_}i = \frac{Y_0\left(Y_{\rm in\_odd} - Y_{\rm in\_even\_}i\right)}{\left(Y_0 + Y_{\rm in\_odd}\right)\left(Y_0 + Y_{\rm in\_even\_}i\right)}, \tag{3b}$$

where $Y_0 = 1/Z_0$, Z_0 is the port impedance. According to Equations (2a), (2b), and (3b), the $S_{21\_}i$ can be derived as

$$S_{21\_}i = \frac{X_{1i} + {\rm j}X_{2i}}{X_{3i} + {\rm j}X_{4i}}. \tag{4}$$

Then, the GD of the proposed circuit can be obtained as

$$\tau_i = -\frac{d\angle S_{21\_}i}{d\omega} = \frac{X'_{1i}X_{2i} - X_{1i}X'_{2i}}{X_{1i}^2 + X_{2i}^2} - \frac{X'_{3i}X_{4i} - X_{3i}X'_{4i}}{X_{3i}^2 + X_{4i}^2}. \tag{5}$$

The values of X_{1i}, X_{2i}, X_{3i}, X_{4i}, X'_{1i}, X'_{2i}, X'_{3i}, and X'_{4i} are given in the Appendix.

In this design, $\theta_{\rm m}$, θ_0, θ_1, and θ_2 are all fixed to $\pi/2$ at the center frequency $f_0 = (f_1 + f_2)\ /\ 2$, where f_1 is the lower working frequency and f_2 is the higher working frequency.

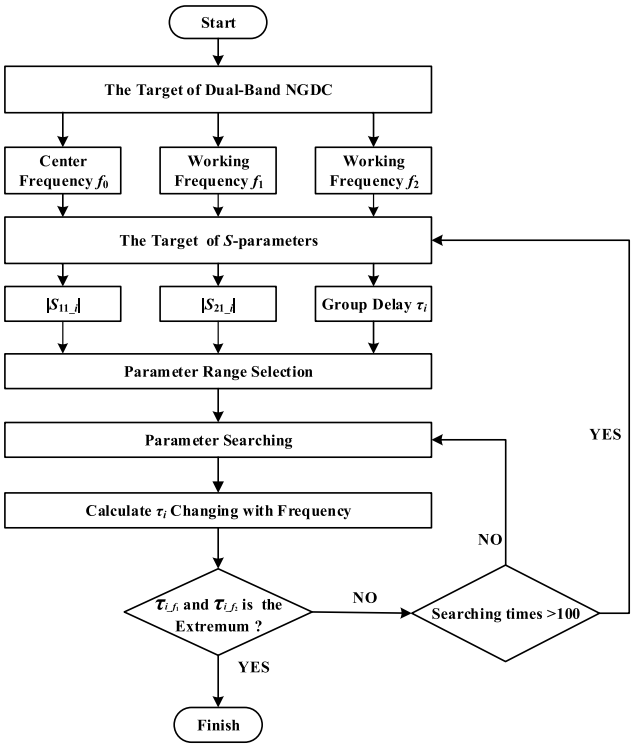

FIGURE 3. The flow chart of the proposed dual-band NGDC design.

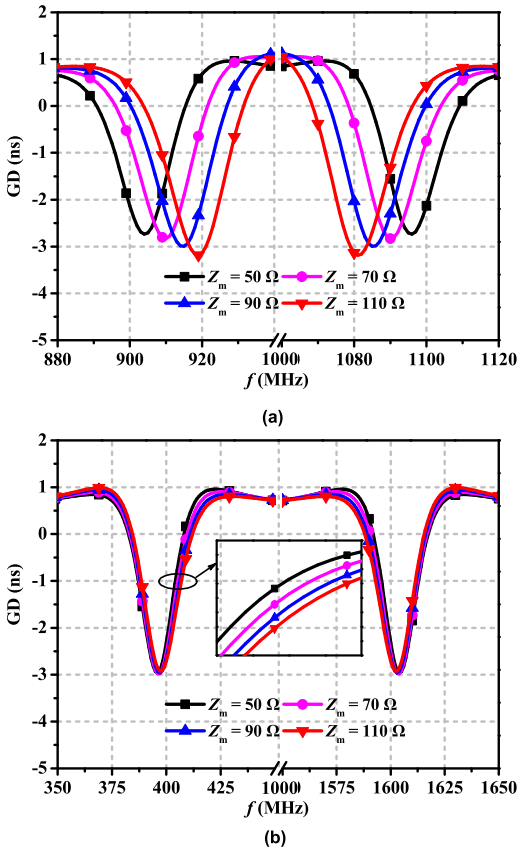

FIGURE 4. Effect of Z_m on the frequency ratio of the proposed dual-band NGDC. (a) open-circuit stub. (b) short-circuit stub.

So the variables to be solved are Z, k, Z_1 (or Z_2), Z_m, R_m, and R. Once the f_0, f_1 and f_2 are selected, Equations (3a), (3b), and (5) can be used to calculate the circuit parameters. By setting the target values ($|S_{11\_i}|$, $|S_{21\_i}|$, and τ_i at two working frequencies), six equations are obtained. And the number of variables to be solved is also six. Due to the closed-form equations are very complex, it is difficult to get the concrete expression of each variable. Thus, an optimization algorithm is utilized to solve the closed-form equations. In this paper, the cuckoo search algorithm [32] is adopted to solve the parameters. In order to use the algorithm, the problem of solving nonlinear equations first should be transformed into solving the optimal value. So the six equations need to be converted into a function as

$$G(X) = |g_1(X)| + |g_2(X)| + |g_3(X)| + |g_4(X)| + |g_5(X)| + |g_6(X)|. \quad (6)$$

The subfunctions in Equation (6) are shown as

$$\begin{cases} g_1(X) = \left|S_{11\_i}(X)\right|_{f=f_1}\Big| \\ g_2(X) = \left|S_{11\_i}(X)\right|_{f=f_2}\Big| \\ g_3(X) = \left|S_{21\_i}(X)\right|_{f=f_1}\Big| - M_1 \\ g_4(X) = \left|S_{21\_i}(X)\right|_{f=f_2}\Big| - M_2 \\ g_5(X) = \tau_i(X)|_{f=f_1} - N_1 \\ g_6(X) = \tau_i(X)|_{f=f_2} - N_2, \end{cases} \quad (7)$$

where X is a row vector consisting of the six variables, M_1 and N_1 are the target values of $|S_{21\_i}|$, and τ_i at f_1, M_2 and N_2 are the target values of $|S_{21\_i}|$, and τ_i at f_2. To realize the input- and output-port matching, the condition that $|S_{11\_i}| = 0$ must be satisfied at the corresponding working frequency. So when $G(X)$ approaches to 0, the values of variables can be obtained. For the selection of the circuit structure, it needs to be analyzed according to the frequency ratio. This problem will be explained in detail in section III. And then, based on the requirement of the algorithm, the range of variables should be given. Fortunately, the accuracy of the cuckoo search algorithm does not depend on the range of variables, so the range can be selected according to the characteristic impedance of the microstrip lines that can be realized. Finally, the variable values can be obtained by the cuckoo search algorithm.

To summarize, a flow chart of the proposed design is shown in Fig. 3. The first step is to determine the targets of frequency, the S-parameters and the GD. Then based on the impedance range of the realizable microstrip lines, the variable interval should be given. After that, the variable values under the corresponding targets can be solved using the algorithm. But in some cases, the solved GD is not the extremum in the frequency range, so an additional judgment is needed.

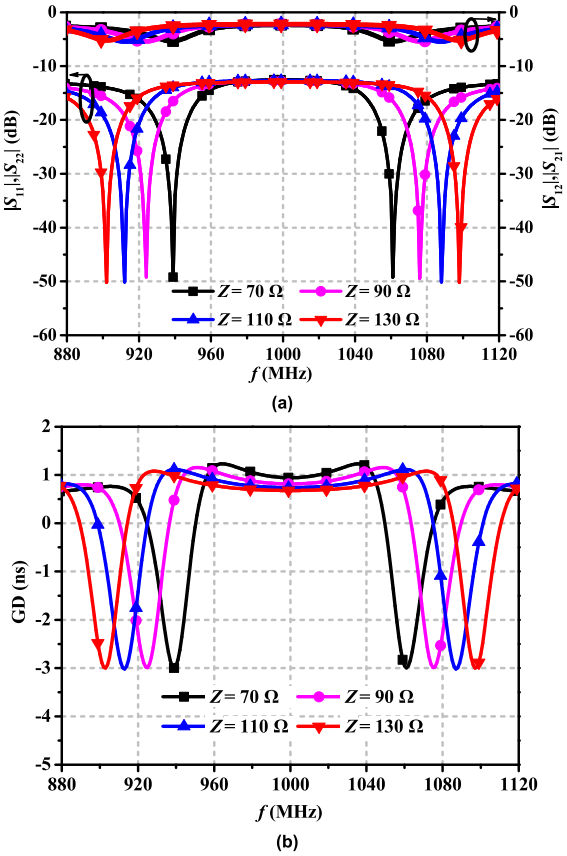

FIGURE 5. Effect of Z on the frequency ratio of the proposed dual-band NGDC. (a) S-parameters. (b) GD.

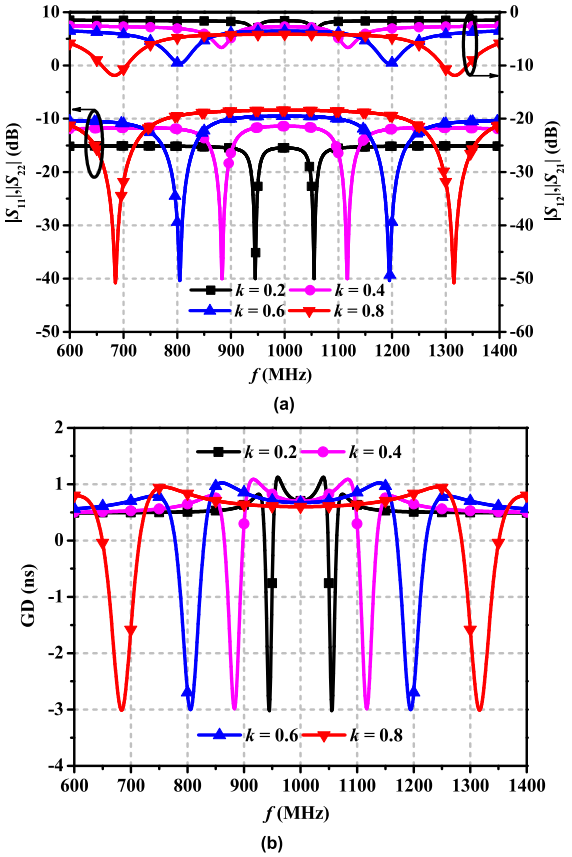

FIGURE 6. Effect of k on the frequency ratio of the proposed dual-band NGDC. (a) S-parameters. (b) GD.

If the GD is the extremum, the program finishes, otherwise search again. Due to the inherent attenuation of the actual circuit and the GD characteristics, there will be a minimum IL under a fixed GD. When the target of $|S_{21\_i}|$ is lower than its extremum, there is no solution. Therefore, a decision box is added to control this situation. If the solutions cannot be available after more than 100 searching times, the search ends. In this case, the requirements for τ_i and $|S_{21\_i}|$ need a compromise.

III. ANALYSIS OF THE PROPOSED DUAL-BAND NGD CIRCUIT

In this part, the variation of Z_m, Z, k_0, Z_i $(i = 1, 2)$ with the frequency ratio is introduced. If the center frequency changes, the design parameters may need to change, but the overall trend is still the same. Therefore, the solutions can be used to guide the selection of the circuit structure.

The changes in GD with frequency under different Z_m are shown in Fig. 4. And the other design parameters remain fixed. As can be seen, whether it is the structure of open-circuited stub or short-circuited stub, the effect of Z_m on the frequency ratio is small, so it is not discussed later.

A. FREQUENCY RATIO OF DUAL-BAND NGDC WITH OPEN-CIRCUITED STUB

To discuss the relationship between the characteristic parameters of the microstrip lines and the frequency ratio, the target values τ_1, $|S_{11\_1}|$ and $|S_{22\_1}|$ are fixed. Fig. 5 shows the S-parameters and GD with the change of Z. The frequency ratio is proportional to Z remaining the bandwidth of GD < 0 and $|S_{21\_1}|$ unchanged at f_1 and f_2. The analysis of k is given in Fig. 6. As k increases the frequency ratio and the NGD bandwidth are expanding while $|S_{21\_1}|$ is decreasing, and the change is obvious. So the choice of k needs a consideration. If a wide bandwidth is needed with a small frequency ratio, the $|S_{21\_1}|$ needs to lower. And Fig. 7 gives the effect of Z_1 on the frequency ratio. With the increase of Z_1, two NGD working frequencies are getting closer, and there is a slight reduction in NGD bandwidth and $|S_{21\_1}|$. Based on the above analysis of the frequency ratio, the minimum of the frequency ratio can be obtained under larger Z_1 along with smaller Z and k. On the contrary, the maximum of the frequency ratio can be obtained. So, the extreme values of the frequency ratio can be calculated under the condition that the microstrip circuit can be implemented with the common printed circuit board (PCB) fabrication technology. In this analysis, the values are calculated with fixed τ_1 of -3 ns and $|S_{11\_1}|$ of

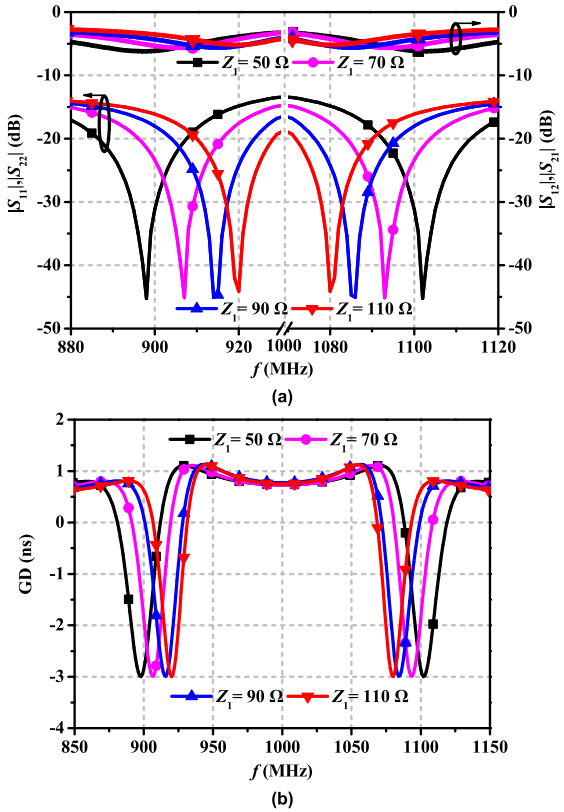

FIGURE 7. Effect of Z_1 on the frequency ratio of the proposed dual-band NGDC. (a) *S*-parameters. (b) GD.

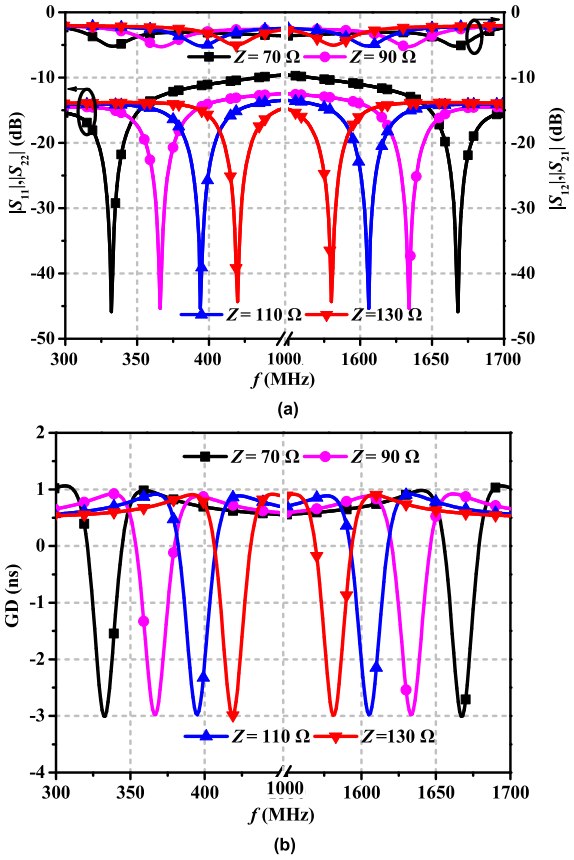

FIGURE 8. Effect of Z on the frequency ratio of the proposed dual-band NGDC. (a) *S*-parameters. (b) GD.

TABLE 1. Design parameters of the dual-band NGDC with open-circuited stub under the extreme values of frequency ratio.

n^*	Z (Ω)	k	Z_1 (Ω)	Z_m (Ω)	R (Ω)	R_m (Ω)
1.095	88.2	0.2127	144.3	102.8	10.8	76.3
2.205	125.5	0.6892	21.2	59.5	31.3	100.4

n^* represents the frequency ratio

TABLE 2. Design parameters of the dual-band NGDC with short-circuited stub under the extreme values of frequency ratio.

n	Z (Ω)	k	Z_2 (Ω)	Z_m (Ω)	R (Ω)	R_m (Ω)
2.095	120.5	0.1621	22.0	82.8	5.7	65.0
6.297	82.2	0.5936	149.8	42.9	30.0	123.7

−40 dB. Table 1 shows two sets of design parameters of the proposed dual- band NGDC with the open-circuited stub for the extreme frequency ratios of 1.095 and 2.205. It means that the frequency ratio can change from 1.095 to 2.205. If the chosen GD is different from this example, the frequency ratio may have slight changes.

B. FREQUENCY RATIO OF DUAL-BAND NGDC WITH SHORT-CIRCUITED STUB

In this part, the same approach will be taken to discuss the relationship between the frequency ratio and characteristic parameters of the microstrip lines. And in order to be consistent with part *A*, the values are still solved with fixed τ_2, $|S_{11\_2}|$ and $|S_{22\_2}|$. Fig. 8 shows the effect of Z on the frequency ratio. The frequency ratio is inversely proportional to Z. And the NGD bandwidth and $|S_{21\_2}|$ keep unchanged at f_1 and f_2. The analysis of k is provided in Fig. 9. The frequency ratio and the NGD bandwidth are both proportional to k. And $|S_{21\_2}|$ is decreasing as k rises. And Fig. 10 shows the *S*-parameters and GD with the change of Z_2. With the increase of Z_2, the frequency ratio is increasing, and there is also a slight reduction in NGD bandwidth and $|S_{21\_2}|$. According to the analysis of the frequency ratio, the minimum value of the frequency ratio can be obtained with larger Z as well as smaller k and Z_2. On the contrary, the maximum value of the frequency ratio can be obtained. In this analysis, the values are calculated under $\tau_2 = -3$ ns and $|S_{11\_2}| = -40$ dB. Table 2 displays two sets of design parameters of the dual-band NGDC with the short-circuited stub. The minimum and maximum frequency ratio is 2.095 and 6.297, respectively.

IV. EXPERIMENTAL VERIFICATION

Based on the derivation and numeric analysis, three dual-band NGD microwave circuits' prototypes with different

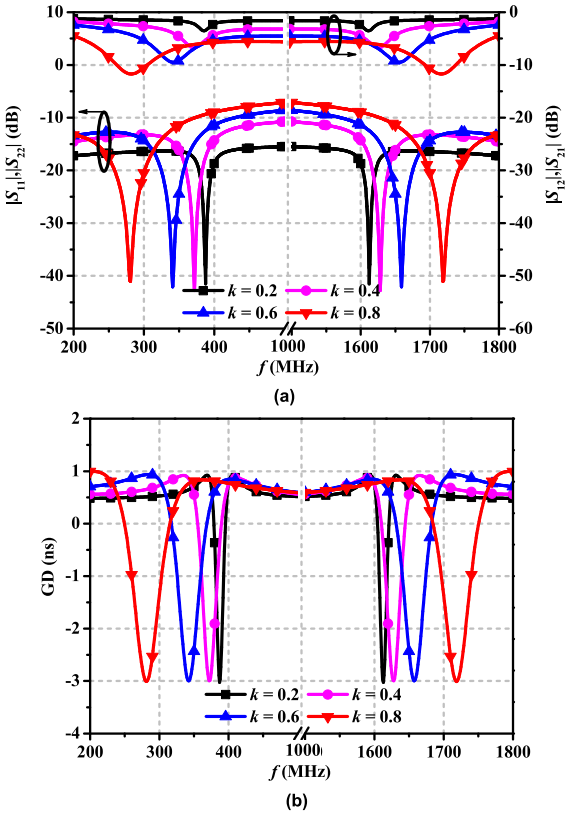

FIGURE 9. Effect of k on the frequency ratio of the proposed dual-band NGDC. (a) S-parameters. (b) GD.

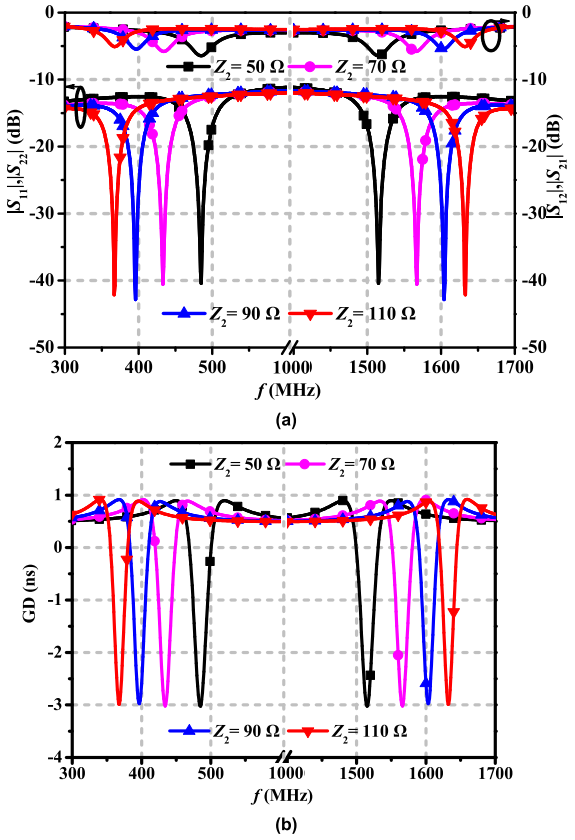

FIGURE 10. Effect of Z_2 on the frequency ratio of the proposed dual-band NGDC. (a) S-parameters. (b) GD.

frequency ratio are designed for demonstration. These prototypes are simulated and optimized in the HFSS EM software. The used substrates are F4B with a thickness of 1.5 mm, the dielectric constant of 2.55, and a loss tangent of 0.003. And an Agilent N5230A network analyzer is used for measurements. The desired frequency ratios are 1.105, 3 and 5.667 with the center frequency of 1 GHz. And the τ_i is set at -3 ns and the $|S_{11\_i}|$ is set as -40 dB on the desired frequency.

A. THE DUAL-BAND NGDC (A) WITH n = 1.105

In the case of $n = 1.105$, f_1 is 950 MHz, and f_2 is 1050 MHz. And the circuit is the one with the open-circuited stub. The $|S_{21\_1}|$ is set as -3.5 dB. Fig. 11 shows the layout of the proposed circuit. And based on the Equations (3a), (3b), (5) and the cuckoo search algorithm, the design parameters are obtained as $Z = 72.3\ \Omega$, $k = 0.2633$, $Z_m = 117.3\ \Omega$, $Z_1 = 122.6\ \Omega$, $R_m = 129.2\ \Omega$, and $R = 11.8\ \Omega$. Using the transmission line synthesis tool *ADS Linecalc*, the physical dimensions of transmission lines are calculated. But they are theoretical values without considering the discontinuous interfaces. After optimizing by HFSS, the final dimensions are $w_0 = 3.9$ mm, $l_0 = 15$ mm, $w_m = 0.7$ mm, $l_m = 56.5$ mm, $w_1 = 0.7$ mm, $l_1 = 52.7$ mm, $w = 1.9$ mm, $s = 0.64$ mm, $l_2 = 18.4$ mm, $l_3 = 16.9$ mm, $l_4 = 40.24$ mm, $d = 1$ mm, $R_m = 130\ \Omega$, and $R = 9.1\ \Omega$. Because of the extra

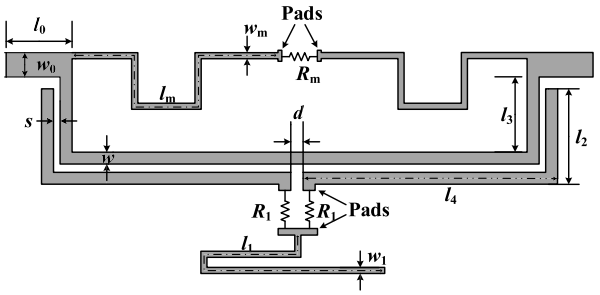

FIGURE 11. Layout of the proposed dual-band NGDC (A) with $n = 1.105$.

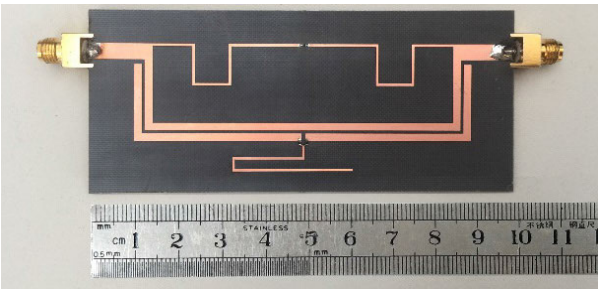

FIGURE 12. Photograph of the proposed dual-band NGDC (A) with $n = 1.105$.

loss caused by the substrate and copper strip, the resistance R is smaller than the theoretical calculation. The photograph of the fabricated dual-band NGDC with $n = 1.105$ is shown

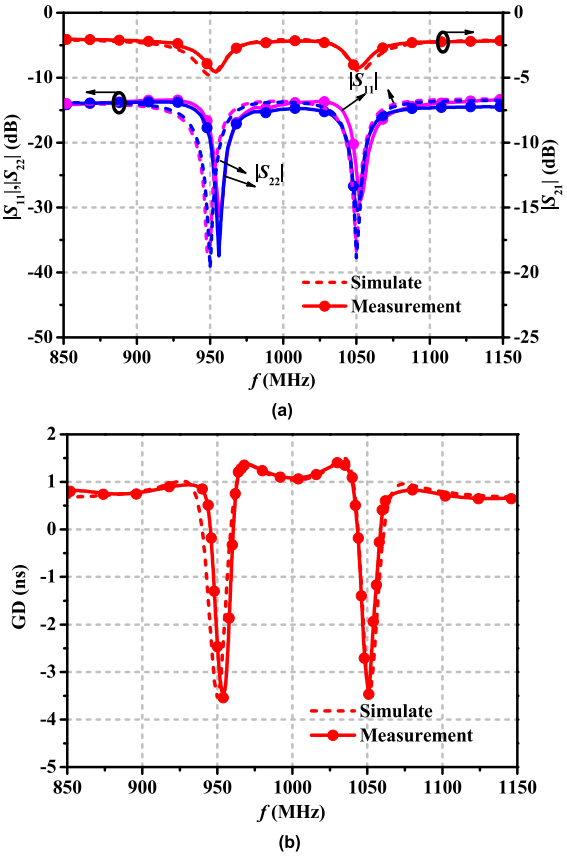

FIGURE 13. Simulation and measured results of the proposed dual-band NGDC (A) with $n = 1.105$. (a) S-parameters. (b) GD.

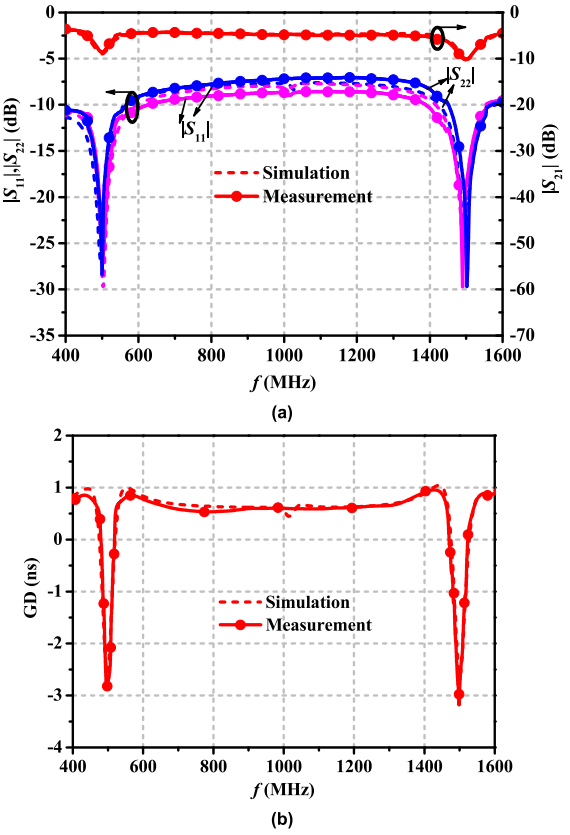

FIGURE 16. Simulation and measured results of the proposed dual-band NGDC (B) with $n = 3$. (a) S-parameters. (b) GD.

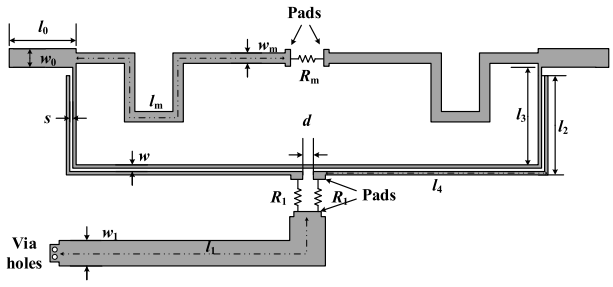

FIGURE 14. Layout of the proposed dual-band NGDC (B) with $n = 3$.

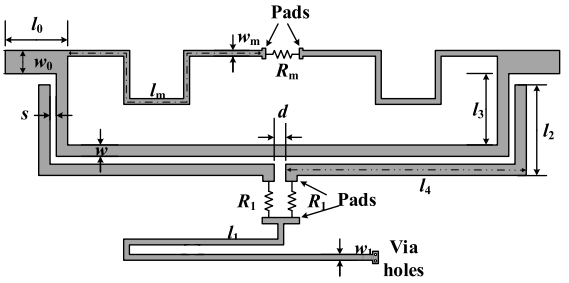

FIGURE 17. Layout of the proposed dual-band NGDC (C) with $n = 5.667$.

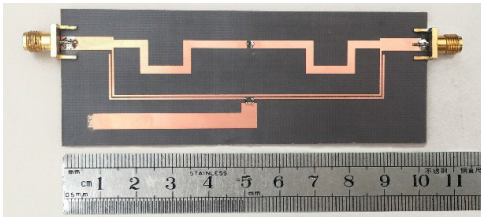

FIGURE 15. Photograph of the proposed dual-band NGDC (B) with $n = 3$.

in Fig. 12. The overall circuit dimension is 40 mm × 98 mm. (Around $0.19\lambda_g \times 0.47\lambda_g$, where λ_g is the guided wavelength of 50-Ω TLs at the center frequency.)

Fig. 13 shows the measured results of S-parameters and GD, along with simulated ones for comparison. For the f_1 of 954 MHz, the measured GD and $|S_{21\_1}|$ are −3.54 ns and −4.53 dB, respectively. The NGD fractional bandwidth (FBW) is 1.57% from 946 to 961 MHz, and the input/output return loss (RL) is better than 16.6 dB in the NGD bandwidth with a maximum RL of 27.2 dB. For the f_2 of 1051 MHz, the measured GD and $|S_{21\_1}|$ are −3.47 ns, and −4.24 dB, respectively. The NGD FBW is 1.33% from 1044 to 1058 MHz, and the input/output RL is better than 20.1 dB in the NGD bandwidth with a maximum RL of 32.3 dB.

TABLE 3. Performance comparison.

References	f(GHz)		GD (ns)		NGD FBW (%)		IL (dB)		RL (dB)		FOM		Frequency ratio	Circuit size ($\lambda_g \times \lambda_g$,)
	f_1	f_2	f_1	f_2	f_1	f_2	f_1	f_2	f_1	f_2	f_1	f_2		
[24]	2.140	3.500	-3.00	-3.10	8.41	5.14	34.2	34.9	17.0	17.0	0.0105	0.0100	1.0-3.0	0.09 × 1.80
[25]	3.500	5.150	-4.54	-4.20	3.43	1.94	47.4	38.8	-	-	0.0023	0.0048	1.5	0.36 × 0.64
[26]	3.500	5.200	-5.00	-5.00	5.71	5.77	13.0	19.5	-	-	0.2237	0.1589	1.5	0.60 × 0.64
[27]	0.667	1.377	-1.19	-1.19	34.60	16.50	18.2	18.2	24.8	24.7	0.0338	0.0332	1.16-2.06	0.13 × 0.27
[28]	0.660	1.390	-1.03	-1.03	35.2	16.6	16.9	16.9	18.4	17.6	0.0338	0.0332	2.1	0.13 × 0.27
This work (A)	**0.954**	**1.501**	**-3.54**	**-3.47**	**1.57**	**1.33**	**4.5**	**4.2**	**27.2**	**32.3**	**0.0315**	**0.0457**		**0.19 × 0.47**
This work (B)	**0.496**	**1.499**	**-2.93**	**-3.05**	**7.66**	**3.67**	**8.3**	**10.2**	**23.3**	**25.4**	**0.0426**	**0.0519**	**1.1-6.3**	**0.19 × 0.50**
This work (C)	**0.300**	**1.704**	**-3.57**	**-3.21**	**5.00**	**1.58**	**4.6**	**5.3**	**25.7**	**28.5**	**0.0315**	**0.0535**		**0.19 × 0.48**

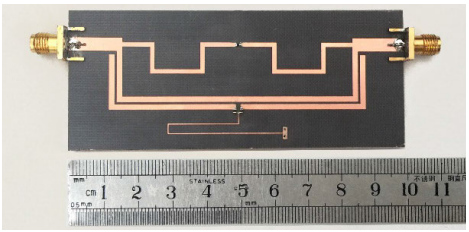

FIGURE 18. Photograph of the proposed dual-band NGDC (C) with $n = 5.667$.

B. THE DUAL-BAND NGDC (B) WITH n = 3

In this instance, n is selected as 3. So f_1 is 500 MHz, and f_2 is 1500 MHz. And the circuit is the one with the short-circuited stub. The $|S_{21\_2}|$ is set as −9 dB. Fig. 14 shows the layout of the proposed circuit. And then the design parameters are $Z = 104.3\ \Omega$, $k = 0.4471$, $Z_m = 69.3\ \Omega$, $Z_2 = 40.1\ \Omega$, $R_m = 114.4\ \Omega$, and $R = 17.5\ \Omega$. After optimizing by HFSS, the final dimensions are $w_0 = 3.9$ mm, $l_0 = 15$ mm, $w_m = 2.4$ mm, $l_m = 55.1$ mm, $w_1 = 4.7$ mm, $l_1 = 51.5$ mm, $w = 0.6$ mm, $s = 0.3$ mm, $l_2 = 13.5$ mm, $l_3 = 13.6$ mm, $l_4 = 40.9$ mm, $d = 1$ mm, $R_m = 110\ \Omega$, and $R = 15\ \Omega$. The photograph of the fabricated dual-band NGD circuit with $n = 3$ is shown in Fig. 15. The overall circuit dimension is 40 mm × 103 mm (Around $0.19\lambda_g \times 0.50\lambda_g$).

Fig. 16 shows the measured results of S-parameters and GD, along with simulated ones for comparison. For the lower band with f_1 of 496 MHz, the measured GD and $|S_{21\_2}|$ are −2.93 ns and −8.35 dB, respectively. The NGD FBW is 7.66% from 480 to 518 MHz, and the input/output RL is better than 15.6 dB in the NGD bandwidth with a maximum RL of 23.3 dB. For the upper band with f_2 of 1499 MHz, the measured GD and $|S_{21\_2}|$ are −3.05 ns, and −10.2 dB, respectively. The NGD FBW is 3.67% from 1470 to 1525 MHz, and the input/output RL is better than 15.5 dB in the NGD bandwidth with a maximum RL of 25.4 dB.

C. THE DUAL-BAND NGDC (C) WITH n = 5.667

In this case, n is 5.667, f_1 is 300 MHz, and f_2 is 1700 MHz. And the circuit is the one with the short-circuited stub. The $|S_{21\_2}|$ is set as −5 dB. Fig. 17 shows the layout of the proposed circuit. After the calculation, the design parameters

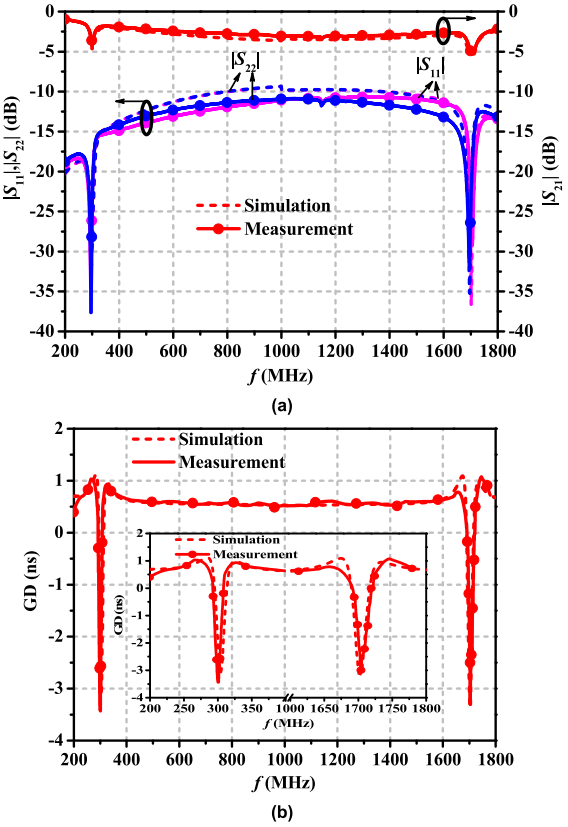

FIGURE 19. Simulation and measured results of the proposed dual-band NGDC (C) with $n = 5.667$. (a) S-parameters. (b) GD.

are $Z = 81.2\ \Omega$, $k = 0.3573$, $Z_m = 64.7\ \Omega$, $Z_2 = 144.4\ \Omega$, $R_m = 127.8\ \Omega$, and $R = 17.7\ \Omega$. After optimizing the final dimensions are $w_0 = 3.9$ mm, $l_0 = 15$ mm, $w_m = 1.3$ mm, $l_m = 49.5$ mm, $w_1 = 0.3$ mm, $l_1 = 58.5$ mm, $w = 1.6$ mm, $s = 0.6$ mm, $l_2 = 15.8$ mm, $l_3 = 14.6$ mm, $l_4 = 36.2$ mm, $d = 1$ mm, $R_m = 150\ \Omega$, and $R = 12\ \Omega$. The photograph of the fabricated dual-band NGD circuit with $n = 5.667$ is shown in Fig. 18. The overall circuit dimension is 40 mm × 99 mm. (Around $0.19\lambda_g \times 0.48\lambda_g$.)

Fig. 19 shows the measured results of S-parameters and GD, along with simulated ones for comparison. In Fig. 19,

for the f_1 of 300 MHz, the measured GD and $|S_{21\_2}|$ are −3.57 ns and −4.6 dB, respectively. The NGD FBW is 5.00% from 293 to 308 MHz, and the input/output RL is better than 17.5 dB in the NGD bandwidth with a maximum RL of 25.7 dB. For the f_2 of 1704 MHz, the measured GD and $|S_{21\_2}|$ are −3.21 ns, and −5.3 dB, respectively. The NGD FBW is 1.58% from 1693 to 1720 MHz, and the input/output RL is better than 18.5 dB in the NGD bandwidth with a maximum RL of 28.5 dB.

V. DISCUSSION

In Figs. 13, 16, and 19, good agreements can be obtained among the simulated and measured results. However, it can be noted that measured loss is larger than that of the simulated results. This is mainly caused by the lossy substrate and copper strip. And the measured GD is slightly lower than simulated. This is due to the tolerance of manufacture. Table 3 shows the comparison of the proposed NGDC with previous works. The proposed NGDC can achieve a wider frequency ratio range than that in [24]–[28]. And it has lower IL and better RL performance than that in [24]–[28]. Besides [26], the proposed NGDC has a better figure of merit (FOM) which can be defined as [33], [34]

$$\mathrm{FOM} = |\tau\,(f)| \times \mathrm{BW}_{\mathrm{NGD}} \times |S_{21}\,(f)|\,. \tag{8}$$

Except for [27], [28], the circuit size of the proposed NGDC is smaller than all the previous works.

VI. CONCLUSION

In this paper, a compact dual-band NGDC has been presented. The closed-form analytical equations have been derived to guide the design. And the characteristic parameters of the microstrip lines that influence the frequency ratio have been investigated. For demonstration, three dual-band NGDCs with a frequency ratio of 1.105, 3, and 5.667 have been designed, fabricated, and measured at the center frequency of 1 GHz. The proposed NGDC has wider frequency ratio range, lower IL and better RL performance. In addition, its size is also small. So it can be applied in various microwave circuits and systems.

APPENDIX

Because the electrical length and GD of the transmission line are frequency dependent, the equations of them are given as

$$\theta_{\mathrm{m}} = \theta_0 = \theta_1 = \theta_2 = \frac{\pi}{2} \times \frac{f}{f_0}, \tag{A1}$$

$$\tau_{\mathrm{m}} = \frac{\theta_{\mathrm{m}}}{\omega_0}, \quad \tau_0 = \frac{\theta_0}{\omega_0}, \ \tau_1 = \frac{\theta_1}{\omega_0}, \ \tau_2 = \frac{\theta_2}{\omega_0}, \tag{A2}$$

where f_0 is the center frequency, $\omega_0 = 2\pi f_0$.

The values of A_1, A_2, A_{3i} and A_{4i} in Equation (2) are given as follow:

$$A_1 = \frac{\left(R_{\mathrm{m}}/2\right)\left(1+\tan^2\theta_{\mathrm{m}}\right)}{R_{\mathrm{m}}^2/4 + Z_{\mathrm{m}}^2\tan^2\theta_{\mathrm{m}}}, \tag{A3}$$

$$A_2 = \frac{\left(R_{\mathrm{m}}^2/4 - Z_{\mathrm{m}}^2\right)\tan\theta_{\mathrm{m}}}{Z_{\mathrm{m}}\left(R_{\mathrm{m}}^2/4 + Z_{\mathrm{m}}^2\tan^2\theta_{\mathrm{m}}\right)} - \frac{2}{(Z_{0e}+Z_{0o})\cot\theta_0}, \tag{A4}$$

$$A_{3i} = \frac{a_1a_{3i} + a_{2i}a_4}{(a_1+a_4a_5)^2 + (a_{2i}+a_{3i}a_5)^2} \quad (i=1,2)\,, \tag{A5}$$

$$A_{4i} = \frac{a_1a_4 - a_{2i}a_{3i} - a_4^2a_5 - a_{3i}^2a_5}{(a_1-a_4a_5)^2 + (a_{2i}+a_{3i}a_5)^2} + \frac{1}{Z_{\mathrm{m}}\tan\theta_{\mathrm{m}}}, \tag{A6}$$

where

$$a_1 = R(Z_{0e}-Z_{0o})/2, \tag{A7}$$

$$a_{21} = \frac{(Z_{0e}-Z_{0o})^2\tan\theta_0}{4} - \frac{(Z_{0e}-Z_{0o})\,(Z_{0o}\cot\theta_0 + 2Z_1\cot\theta_1)}{2}, \tag{A8}$$

$$a_{22} = \frac{(Z_{0e}-Z_{0o})^2\tan\theta_0}{4} - \frac{(Z_{0e}-Z_{0o})\,(Z_{0o}\cot\theta_0 - 2Z_2\tan\theta_2)}{2}, \tag{A9}$$

$$a_{31} = (Z_{0e}+Z_{0o})/2 + 2Z_1\cot\theta_1\tan\theta_0, \tag{A10}$$

$$a_{32} = (Z_{0e}+Z_{0o})/2 - 2Z_2\tan\theta_2\tan\theta_0, \tag{A11}$$

$$a_4 = R\tan\theta_0, \tag{A12}$$

$$a_5 = -Z_{0o}\cot\theta_0. \tag{A13}$$

The values of X_{1i}, X_{2i}, X_{3i}, X_{4i}, X'_{1i}, X'_{2i}, X'_{3i}, and X'_{4i} used in the Equation (4) and Equation (5) are given as follow:

$$X_{1i} = Y_0\,(A_1 - A_{3i})\,, \tag{A14}$$

$$X_{2i} = Y_0\,(A_2 - A_{4i})\,, \tag{A15}$$

$$X_{3i} = Y_0^2 + Y_0\,(A_1 + A_{3i}) + A_1A_{3i} - A_2A_{4i}, \tag{A16}$$

$$X_{4i} = Y_0\,(A_2 + A_{4i}) + A_2A_{3i} + A_1A_{4i}, \tag{A17}$$

$$X'_{1i} = Y_0\left(A'_1 - A'_{3i}\right), \tag{A18}$$

$$X'_{2i} = Y_0\left(A'_2 - A'_{4i}\right), \tag{A19}$$

$$X'_{3i} = Y_0\left(A'_1 + A'_{3i}\right) + A'_1A_{3i} + A_1A'_{3i} - A'_2A_{4i} - A_2A'_{4i}, \tag{A20}$$

$$X'_{4i} = Y_0\left(A'_2 + A'_{4i}\right) + A'_2A_{3i} + A_2A'_{3i} + A'_1A_{4i} + A_1A'_{4i}, \tag{A21}$$

where

$$A'_1 = \frac{\left[\begin{array}{l} R_{\mathrm{m}}\tan\theta_{\mathrm{m}}\left(1+\tan^2\theta_{\mathrm{m}}\right)\tau_{\mathrm{m}}\left(R_{\mathrm{m}}^2/4 + Z_{\mathrm{m}}^2\tan^2\theta_{\mathrm{m}}\right) \\ -2\left(R_{\mathrm{m}}/2\right)\left(1+\tan^2\theta_{\mathrm{m}}\right)^2 Z_{\mathrm{m}}^2\tan\theta_{\mathrm{m}}\tau_{\mathrm{m}} \end{array}\right]}{\left(R_{\mathrm{m}}^2/4 + Z_{\mathrm{m}}^2\tan^2\theta_{\mathrm{m}}\right)^2}, \tag{A22}$$

$$A'_2 = \left[\begin{array}{l} \left(R_{\mathrm{m}}^2/4 - Z_{\mathrm{m}}^2\right)\left(1+\tan^2\theta_{\mathrm{m}}\right)\tau_{\mathrm{m}}\left(R_{\mathrm{m}}^2/4 + Z_{\mathrm{m}}^2\tan^2\theta_{\mathrm{m}}\right) \\ -2\left(R_{\mathrm{m}}^2/4 - Z_{\mathrm{m}}^2\right)\tan^2\theta_{\mathrm{m}}Z_{\mathrm{m}}^2\left(1+\tan^2\theta_{\mathrm{m}}\right)\tau_{\mathrm{m}} \end{array}\right] \times \frac{1}{Z_{\mathrm{m}}\left(R_{\mathrm{m}}^2/4 + Z_{\mathrm{m}}^2\tan^2\theta_{\mathrm{m}}\right)^2} + \frac{2\left(1+\cot^2\theta_0\right)\tau_0}{Z_{0e}+Z_{0o}},$$

(A23)

$$A'_{3i} = \frac{\left\{\begin{array}{l}\left(\begin{array}{l}a'_1a_{3i}+a_1a'_{3i}\\+a'_{2i}a_4+a_{2i}a'_4\end{array}\right)\left[\begin{array}{l}(a_1-a_4a_5)^2\\+(a_{2i}-a_{3i}a_5)^2\end{array}\right]-\left(\begin{array}{l}a_1a_{3i}\\+a_{2i}a_4\end{array}\right)\\\times\left[\begin{array}{l}2(a_1-a_4a_5)\left(a'_1-a'_4a_5-a_4a'_5\right)\\+2(a_{2i}+a_{3i}a_5)\left(a'_{2i}+a'_{3i}a_5+a_{3i}a'_5\right)\end{array}\right]\end{array}\right\}}{\left[(a_1-a_4a_5)^2+(a_{2i}+a_{3i}a_5)^2\right]^2},$$

(A24)

$$A'_{4i} = \frac{\left\{\begin{array}{l}\left(\begin{array}{l}a'_1a_4+a_1a'_4-a'_{2i}a_{3i}-a_{2i}a'_{3i}\\-2a_4a'_4a_5-a_4^2a'_5-2a_{3i}a'_{3i}a_5-a_{3i}^2a'_5\end{array}\right)\\\times\left[(a_1-a_4a_5)^2+(a_{2i}+a_{3i}a_5)^2\right]\\-\left(a_1a_4-a_{2i}a_{3i}-a_4^2a_5-a_{3i}^2a_5\right)\\\times\left[\begin{array}{l}2(a_1-a_4a_5)\left(a'_1-a'_4a_5-a_4a'_5\right)\\+2(a_{2i}+a_{3i}a_5)\left(a'_{2i}+a'_{3i}a_5+a_{3i}a'_5\right)\end{array}\right]\end{array}\right\}}{\left[(a_1-a_4a_5)^2+(a_{2i}+a_{3i}a_5)^2\right]^2}$$

$$+(1+\tan\theta_{\rm m})\,\tau_{\rm m}/Z_{\rm m}, \tag{A25}$$

$$a'_1 = 0, \tag{A26}$$

$$a'_{21} = \frac{(Z_{0e}-Z_{0o})\left[\begin{array}{l}(Z_{0e}-Z_{0o})\left(1+\tan^2\theta_0\right)\tau_0/2+Z_{0o}\\\times\left(1+\cot^2\theta_0\right)\tau_0+2Z_1\left(1+\cot^2\theta_1\right)\tau_1\end{array}\right]}{2}, \tag{A27}$$

$$a'_{22} = \frac{(Z_{0e}-Z_{0o})\left[\begin{array}{l}(Z_{0e}-Z_{0o})\left(1+\tan^2\theta_0\right)\tau_0/2+Z_{0o}\\\times\left(1+\cot^2\theta_0\right)\tau_0+2Z_2\left(1+\tan^2\theta_2\right)\tau_2\end{array}\right]}{2}, \tag{A28}$$

$$a'_{31} = 2Z_1\left(1+\tan^2\theta_0\right)\cot\theta_1\tau_0-2Z_1\left(1+\cot^2\theta_1\right)\tan\theta_0\tau_1, \tag{A29}$$

$$a'_{32} = -2Z_2\left(1+\tan\theta_0^2\right)\tan\theta_2\tau_0-2Z_2\left(1+\tan^2\theta_2\right)\tan\theta_0\tau_2, \tag{A30}$$

$$a'_4 = R\left(1+\tan^2\theta_0\right)\tau_0, \tag{A31}$$

$$a'_5 = Z_{0o}\left(1+\cot^2\theta_0\right)\tau_0. \tag{A32}$$

REFERENCES

[1] H. Turki, L. Huitema, T. Monediere, B. Lenoir, and C. Breuil, "New concept validation of low-loss dual-band stripline circulator," *IEEE Trans. Microw. Theory Techn.*, vol. 67, no. 3, pp. 845–850, Mar. 2019.

[2] E. Doumanis, L. Guan, G. Goussetis, and D. Ferling, "Dual-band bandpass double ground plane coaxial resonators and filters," *IEEE Trans. Microw. Theory Techn.*, vol. 66, no. 8, pp. 3828–3835, Aug. 2018.

[3] P.-J. Li and T.-L. Wu, "Synthesized method of dual-band common-mode noise absorption circuits," *IEEE Trans. Microw. Theory Techn.*, vol. 67, no. 4, pp. 1392–1401, Apr. 2019.

[4] Y. Park, C.-H. Lee, J. D. Cressler, and J. Laskar, "The analysis of UWB SiGe HBT LNA for its noise, linearity, and minimum group delay variation," *IEEE Trans. Microw. Theory Techn.*, vol. 54, no. 4, pp. 1687–1697, Jun. 2006.

[5] K.-P. Ahn, R. Ishikawa, and K. Honjo, "Group delay equalized UWB InGaP/GaAs HBT MMIC amplifier using negative group delay circuits," *IEEE Trans. Microw. Theory Techn.*, vol. 57, no. 9, pp. 2139–2147, Sep. 2009.

[6] K.-P. Ahn, R. Ishikawa, and K. Honjo, "Low noise group delay equalization technique for UWB InGaP/GaAs HBT LNA," *IEEE Microw. Wireless Compon. Lett.*, vol. 20, no. 7, pp. 405–407, Jul. 2010.

[7] Y. Wu, H. Wang, Z. Zhuang, Y. Liu, Q. Xue, and A. A. Kishk, "A novel arbitrary terminated unequal coupler with bandwidth-enhanced positive and negative group delay characteristics," *IEEE Trans. Microw. Theory Techn.*, vol. 66, no. 5, pp. 2170–2184, May 2018.

[8] F. Wan, X. Miao, B. Ravelo, Q. Yuan, J. Cheng, Q. Ji, and J. Ge, "Design of multi-scale negative group delay circuit for sensors signal time-delay cancellation," *IEEE Sensors J.*, vol. 19, no. 19, pp. 8951–8962, Oct. 2019.

[9] S. Lucyszyn, I. D. Robertson, and A. H. Aghvami, "Negative group delay synthesiser," *Electron. Lett.*, vol. 29, no. 9, p. 798, Apr. 1993.

[10] C. D. Broomfield and J. K. A. Everard, "Broadband negative group delay networks for compensation of microwave oscillators and filters," *Electron. Lett.*, vol. 36, no. 23, p. 1931, 2000.

[11] J. Woodley and M. Mojahedi, "Negative group velocity in left-handed materials," in *Proc. IEEE Antennas Propag. Soc. Int. Symposium. Digest. Held Conjunct: USNC/CNC/URSI North Amer. Radio Sci. Meeting*, vol. 4, Jun. 2003, pp. 643–646.

[12] H. Choi, G. Chaudhary, T. Moon, Y. Jeong, J. Lim, and C. D. Kim, "A design of composite negative group delay circuit with lower signal attenuation for performance improvement of power amplifier linearization techniques," *IEEE MTT-S Int. Microw. Symp. Dig.*, Jun. 2011, pp. 1–4.

[13] G. Chaudhary and Y. Jeong, "Distributed transmission line negative group delay circuit with improved signal attenuation," *IEEE Microw. Wireless Compon. Lett.*, vol. 24, no. 1, pp. 20–22, Jan. 2014.

[14] G. Chaudhary and Y. Jeong, "Low signal-attenuation negative group-delay network topologies using coupled lines," *IEEE Trans. Microw. Theory Techn.*, vol. 62, no. 10, pp. 2316–2324, Oct. 2014.

[15] G. Chaudhary and Y. Jeong, "Transmission-line negative group delay networks with improved signal attenuation," *IEEE Antennas Wireless Propag. Lett.*, vol. 13, pp. 1039–1042, 2014.

[16] G. Chaudhary, Y. Jeong, and J. Im, "A design of reconfigurable negative group delay circuit without external resonators," *IEEE Antennas Wireless Propag. Lett.*, vol. 14, pp. 883–886, 2015.

[17] G. Chaudhary and Y. Jeong, "Transmission-type negative group delay networks using coupled line doublet structure," *IET Microw., Antennas Propag.*, vol. 9, no. 8, pp. 748–754, Jun. 2015.

[18] Y. Wu, Z. Zhuang, H. Wang, and Y. Liu, "Impedance-transforming matched negative group delay circuits with enhanced bandwidth," in *Proc. IEEE Int. Workshop Electromagnetics: Appl. Student Innov. Competition (iWEM)*, May 2016, pp. 1–3.

[19] F. Wan, N. Li, B. Ravelo, Q. Ji, and J. Ge, "S-parameter model of three parallel interconnect lines generating negative group-delay effect," *IEEE Access*, vol. 6, pp. 57152–57159, 2018.

[20] F. Wan, N. Li, B. Ravelo, J. Ge, and B. Li, "Time-domain experimentation of NGD active RC-network cell," *IEEE Trans. Circuits Syst. I, Reg. Papers*, vol. 66, no. 4, pp. 562–566, Apr. 2019.

[21] M. Kandic and G. E. Bridges, "Asymptotic limits of negative group delay in active resonator-based distributed circuits," *IEEE Trans. Circuits Syst. I, Reg. Papers*, vol. 58, no. 8, pp. 1727–1735, Aug. 2011.

[22] F. Wan, T. Gu, B. Ravelo, B. Li, J. Cheng, Q. Yuan, and J. Ge, "Negative group delay theory of a four-port RC-network feedback operational amplifier," *IEEE Access*, vol. 7, pp. 75708–75720, 2019.

[23] F. Wan, N. Li, B. Ravelo, Q. Ji, B. Li, and J. Ge, "The design method of the active negative group delay circuits based on a microwave amplifier and an RL-series network," *IEEE Access*, vol. 6, pp. 33849–33858, 2018.

[24] H. Choi, Y. Jeong, J. Lim, S.-Y. Eom, and Y.-B. Jung, "A novel design for a dual-band negative group delay circuit," *IEEE Microw. Wireless Compon. Lett.*, vol. 21, no. 1, pp. 19–21, Jan. 2011.

[25] G. Chaudhary, Y. Jeong, and J. Lim, "Miniaturized dual-band negative group delay circuit using dual-plane defected structures," *IEEE Microw. Wireless Compon. Lett.*, vol. 24, no. 8, pp. 521–523, Aug. 2014.

[26] H. Taher and R. Farrell, "Dual wide-band miniaturized negative group delay circuit using open circuit stubs," *Microw. Opt. Technol. Lett.*, vol. 60, no. 2, pp. 428–432, Feb. 2018.

[27] T. Shao, S. Fang, Z. Wang, and H. Liu, "A compact dual-band negative group delay microwave circuit," *Radioengineering*, vol. 27, no. 4, pp. 1070–1076, Dec. 2018.
[28] T. Shao, S. Fang, Z. Wang, H. Liu, and S. Fu, "A novel dual-band negative group delay microwave circuit," in *Proc. IEEE Radio Wireless Symposium (RWS)*, Jan. 2019, pp. 1–3.
[29] B. Ravelo and S. De Blasi, "An FET-based microwave active circuit with dual-band negative group delay," *J. Microw., Optoelectronics Electromagn. Appl.*, vol. 10, no. 2, pp. 355–366, Dec. 2011.
[30] G. Matthaei, L. Young, and E. M. T. Jomes, *Microwave Fliters, Impenance-Matching Networks, and Coupling Structures*. North Bergen, NJ, USA: BookMart Press, 1985, pp. 219–227.
[31] J. Hong, *Microstrip Filters for RF/Microwave Applications*, 2nd ed. Hoboken, NJ, USA: Wiley, 2011.
[32] S. Walton, O. Hassan, K. Morgan, and M. R. Brown, "Modified cuckoo search: A new gradient free optimisation algorithm," *Chaos, Solitons Fractals*, vol. 44, no. 9, pp. 710–718, Sep. 2011.
[33] B. Ravelo, "Theory of coupled line coupler-based negative group delay microwave circuit," *IEEE Trans. Microw. Theory Techn.*, vol. 64, no. 11, pp. 3604–3611, Nov. 2016.
[34] Z. Wang, Y. Cao, T. Shao, S. Fang, and Y. Liu, "A negative group delay microwave circuit based on signal interference techniques," *IEEE Microw. Wireless Compon. Lett.*, vol. 28, no. 4, pp. 290–292, Apr. 2018.

YUWEI MENG was born in Liaoning, China. She received the B.Eng. degree in communication engineering from Dalian Maritime University, Liaoning, China, in 2016, where she is currently pursuing the Ph.D. degree. Her current research interests include negative group delay circuit and low-noise amplifier.

ZHONGBAO WANG (Member, IEEE) received the Ph.D. degree in communication and information systems from Dalian Maritime University (DMU), China, in 2012. He is currently an Associate Professor with the School of Information Science and Technology, DMU. From 2014 to 2018, he was a Postdoctoral Fellow with the Beijing University of Posts and Telecommunications. From 2019 to 2020, he is a Visiting Scholar with the Department of Electrical and Computer Engineering, National University of Singapore, Singapore. His current research interests include passive RF components, patch antennas, and microwave technology using artificial intelligence. He has authored or coauthored two books and more than 70 articles in journals and conferences. He is currently serving as a Technical Reviewer for the IEEE TRANSACTIONS ON MICROWAVE THEORY AND TECHNIQUES, the IEEE TRANSACTIONS ON CIRCUITS AND SYSTEMS, the IEEE TRANSACTIONS ON INDUSTRIAL ELECTRONICS, the IEEE MICROWAVE AND WIRELESS COMPONENTS LETTERS, the IEEE ANTENNAS AND WIRELESS PROPAGATION LETTERS, IEEE ACCESS, the *IET Microwaves, Antennas and Propagation*, *Electronics Letters*, *Radioengineering*, the *International Journal of RF and Microwave Computer-Aided Engineering*, and *AEU-International Journal of Electronics and Communications*. He was a recipient of the Best Doctor's Dissertation Award of Liaoning Province, in 2013.

SHAOJUN FANG (Member, IEEE) received the Ph.D. degree in communication and information systems from Dalian Maritime University (DMU), China, in 2001. Since 1982, he has been with DMU, where he is currently the Head Professor with the School of Information Science and Technology. His recent research interests include passive RF components and antennas. He has authored or coauthored four books and more than 100 journal and conference articles. He was a recipient of the Best Doctor's Dissertation Award of Liaoning Province, in 2002, and the Outstanding Teacher Award of the Ministry of Transport of China.

TE SHAO was born in Harbin, China. He received the B.Eng. and M.Eng. degrees in information and communication engineering from Dalian Maritime University, Liaoning, China, in 2013 and 2016, respectively, where he is currently pursuing the Ph.D. degree. His current research interests include negative group delay circuit and linear-phase band-pass filter.

HONGMEI LIU (Member, IEEE) received the Ph.D. degree in communication and information systems from Dalian Maritime University (DMU), China, in 2016. She is currently an Associate Professor with the School of Information Science and Technology, DMU. Her current research interests include passive microwave circuits, reconfigurable RF components, and CP microwave antennas. She was a recipient of the Best Doctor's Dissertation Award of Liaoning Province, in 2017. She is currently serving as a Technical Reviewer for the IEEE TRANSACTIONS ON INDUSTRIAL ELECTRONICS, the *Electronics Letters*, and the *International Journal of RF and Microwave Computer-Aided Engineering*.

ZHINING CHEN (Fellow, IEEE) received the B.Eng., M.Eng., and Ph.D. degrees in electrical engineering from the Institute of Communications Engineering (ICE), Nanjing, China, and the Ph.D. degree from the University of Tsukuba, Ibaraki, Japan.

From 1988 to 1995, he was a Lecturer and later an Associate Professor with ICE, and a Postdoctoral Fellow with Southeast University, Nanjing, China. From 1995 to 1997, he was a Research Assistant and later a Research Fellow with the City University of Hong Kong. In 1997, he was awarded the Japan Society for the Promotion of Science (JSPS) Fellowship to conduct his research at the University of Tsukuba, Japan. In 2001 and 2004, he visited the University of Tsukuba twice under a JSPS Fellowship Program (Senior Fellow). In 2004, he worked as an Academic Visitor with the IBM T. J. Watson Research Center, USA. In 2013, he visited the Laboratoire des Signaux et Systèmes, UMR, CNRS-Supelec-University Paris Sud, Gif-sur-Yvette, France as a Senior DIGITEO Guest Scientist. From 1999 to 2016, he worked with the Institute for Infocomm Research (I2R) as a Principal Scientist, the Head/Manager of the RF & Optical Department, and a Technical Advisor. In 2012, he joined the Department of Electrical and Computer Engineering, National University of Singapore as a tenured Full Professor and currently the Program Director (Industry).

In 2015, he visited the Center for Northeast Asian Studies of Tohoku University, Japan as a Senior Visiting Professor. He was/is holding the concurrent guest professorships at Southeast University (Changjiang Chair Professor), Nanjing University, Tsinghua University, Shanghai Jiao Tong University, Tongji University, the University of Science and Technology of China, Fudan University, Dalian Maritime University, Chiba University, the National Taiwan University of Science and Technology, the South China University of Technology, Shanghai University, the Beijing University of Posts and Telecommunications, Yunnan University, the Beijing Institute of Technology, and the City University of Hong Kong. He is currently serving as the members of the State Key Laboratory of Millimeter-Waves, Southeast University, and also with the State Key Laboratory of Tera-Hertz & Millimeter-Waves, City University of Hong Kong. He has published more than 650 academic articles and five books entitled *Broadband Planar Antennas* (Wiley, 2005), *UWB Wireless Communication* (Wiley, 2006), *Antennas for Portable Devices* (Wiley, 2007), *Antennas for Base Stations in Wireless Communications* (McGraw-Hill, 2009), and *Handbook of Antenna Technologies* (Springer 2016) with 76 chapters as an Editor-in-Chief. He has also contributed the chapters to the books entitled *UWB Antennas and Propagation for Communications, Radar, and Imaging* (Wiley, 2006), *Antenna Engineering Handbook* (McGraw-Hill, 2007), *Microstrip and Printed Antennas* (Wiley, 2010), *Electromagnetics of Body Area Networks* (Wiley, 2016), and *Developments in Antenna Analysis and Design* (IET, 2018). He holds 32 granted/filed patents and completed more than 38 technology licensed deals with industry. He is pioneering in developing small and wideband/UWB antennas, wearable/implanted medical antennas, package antennas, near-field antennas/coils, three-dimensional integrated LTCC arrays, microwave lens antennas, microwave metamaterial/metasurface antennas for communications, sensing, and imaging systems. He is currently more interested in the translational research of metasurfaces into antenna engineering.

Dr. Chen was elevated as the Fellow of the Academy of Engineering, Singapore, in 2019, and a Fellow of the IEEE for contributions to small and broadband antennas for wireless applications in 2007. He was a recipients of the International Symposium on Antennas and Propagation Best Paper Award, in 2010, the CST University Publication Award, in 2008 and 2015, the ASEAN Outstanding Engineering Achievement Award, in 2013, the IES Prestigious Engineering Achievement Award in 2006, 2013 (two awards), and 2014, the I2R Quarterly Best Paper Award, in 2004, and the IEEE iWAT Best Poster Award, in 2005, several technology achievement awards from China from 1990 to 1997, and more than 21 academic awards by the students under his supervision. He has provided 11 local and overseas telecommunications and IT MNCs and SMEs with the technical consultancy service as a Technical Advisor, a Guest Professor, and a Chief Scientist. He is the Founding General Chair of the International Workshop on Antenna Technology (iWAT 2015), the International Symposium on InfoComm & Media Technology in Bio-Medical & Healthcare Applications (IS 3T-in-3A 2010), the International Microwave Forum (IMWF 2010), and the Asia-Pacific Conference on Antennas and Propagation (APCAP 2012). He has been also involved in many international events as a General Chairs, a Chairs, and a members for technical program committees and international advisory committees. He has been invited to deliver over 90 keynote/plenary/invited speeches at international academic and industry events. He served as an Associate Editor for the IEEE TRANSACTIONS ON ANTENNAS AND PROPAGATION and the IEEE Antennas and Propagation Society as a Distinguished Lecturer. He has been serving the IEEE Council on RFID as the Vice President and a Distinguished Lecturer since 2015.